Temperature and pressure effects on the electrochemical CO2 reduction

Vos, R.E.

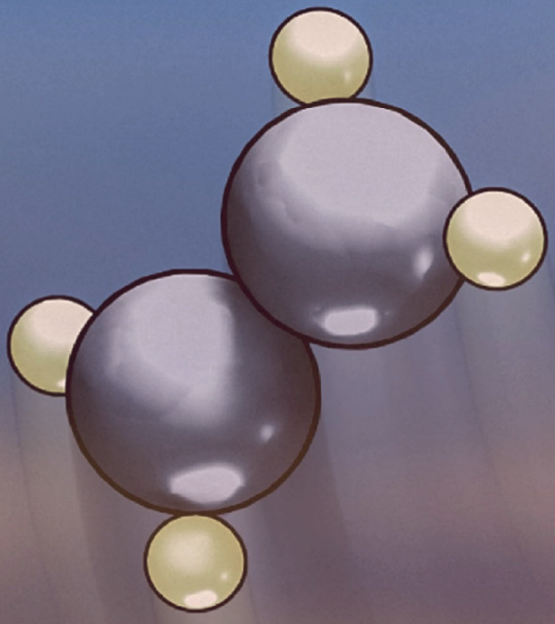

7

Change in the C-C coupling mechanism during CO_2 electroreduction on Cu at elevated temperature and pressure

This chapter is based on R.E. Vos, P. Sun, D. Schauermann, S. R. Hanselman, M.T.M. Koper, in preparation

Abstract

Future practical applications of the electrochemical CO_2 reduction reaction (CO2RR) will likely involve the use of higher pressures and temperatures. However, most research on e.g. the copper-catalyzed CO2RR is typically performed at ambient conditions, and hence the mechanistic conclusions drawn also pertain to these conditions. Using a special high-pressure high-temperature electrochemical cell, we show that on copper electrodes, the C-C coupling mechanism changes from the typical CO dimerization mechanism at low temperatures to a Fischer-Tropsch-like chain growth mechanism at temperatures above 125 °C (requiring higher pressure). Additionally, temperature influences the selectivity more significantly than pressure, however copper stability is compromised at elevated temperatures. The stability can be improved with increasing pressures, which also suppresses the competing hydrogen evolution reaction significantly. These results show that temperature and pressure are crucial parameters to consider in applied and mechanistic studies of the electrochemical reduction of CO_2.

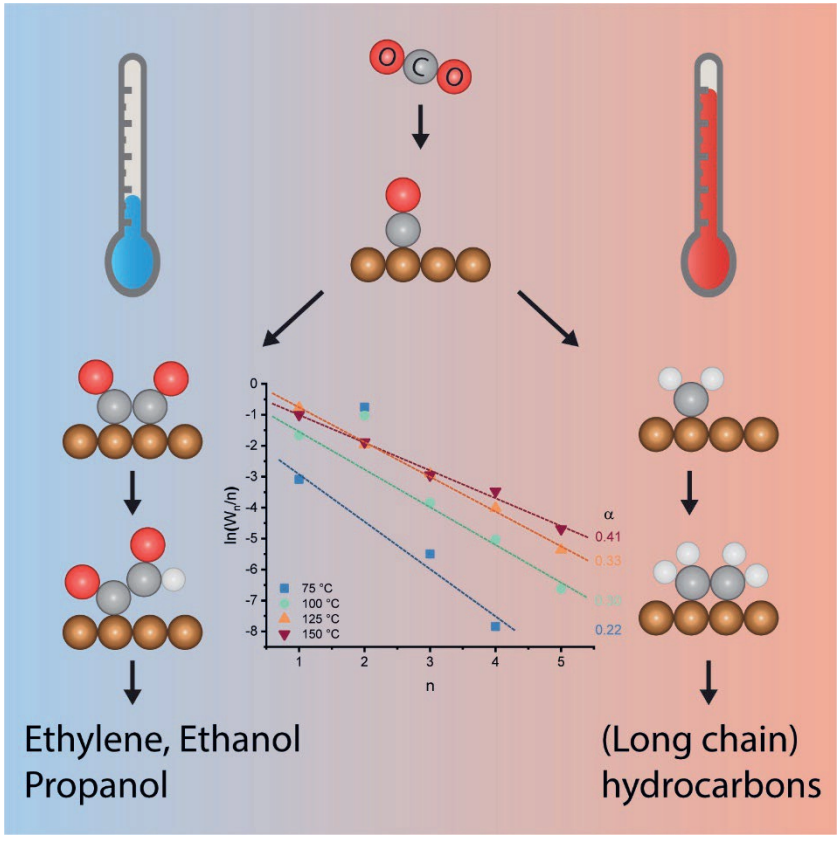

7.1 Introduction

Electrochemical CO_2 reduction (CO2RR) offers an interesting strategy to recycle CO_2 into fuels and chemicals using renewable electricity [1–4]. Copper is a unique catalyst for this reaction, as it is the only catalyst that can make C-C bonds with significant Faradaic efficiencies [5–7]. Multicarbon products in CO2RR are typically formed via a CO dimerization or carbonyl coupling mechanism [8–13], although recently research has provided evidence for a chain growth mechanism as alternative C-C coupling mechanism on for example Ni electrodes[14–17]. Many factors influencing the CO2RR on Cu have been studied, such as morphology [18–21], electrolyte effects [22–25] and electrode potential [7,11,24–26]. Recently, more attention has been given to parameters such as pressure [27–30] and temperature [14,31–34]. Electrochemistry research in general and CO2RR studies specifically are often performed at ambient pressure and temperature and hence conclusions and fundamental insights are drawn at these conditions. However, for practical applications, ambient conditions might not be the most relevant, as industrial electrolyzers typically operate at elevated temperatures [35], for example due to thermal losses [36–38] and/or hot feedstocks. Moreover, pressure and temperature can improve the selectivity and activity of CO2RR [27–29,31,32], open up new mechanistic pathways [30,39] and elevated pressure could enable better integration with up- and downstream processes [30,40,41].

Temperature has a significant effect on the activity and selectivity of CO2RR on Cu at ambient pressure [32]. Below 48 °C, increasing temperature has a positive effect on both the selectivity as activity towards C2+ products, but above 48 °C the competing hydrogen evolution reaction (HER) takes over. Other studies [27–30,40,42–44] have shown that increased CO_2 pressures can suppress the HER, which might mean that the optimum in C2+ selectivity with temperature changes at elevated pressures. Moreover, under elevated pressures the studied temperature window can be increased and experiments in aqueous electrolytes can even be performed above 100 °C. This could bridge the fields of electrocatalysis and thermal catalysis, where C-C bonds are made via a chain growth mechanism in the Fischer-Tropsch reaction [45–47] (although Cu produces mainly methanol in thermal heterogeneous catalysis [48–50]). This raises the question if the electrochemical CO_2 reduction on Cu at high temperatures in aqueous electrolyte is more similar to electrocatalysis at ambient conditions, to thermal catalysis or to neither of them.

Recently, we have developed an electrochemical cell in which both pressure and temperature can be regulated up to 200 °C and 140 bar [51]. In this study, we use this setup to study the combined effect of elevated pressure and temperature and we show a change in the C-C coupling mechanism on copper electrodes above 100

°C, at a pressure of 24 bar. Whereas at low temperatures C-C bonds are mostly formed via the traditional CO dimerization mechanism, at high temperatures the chain growth mechanism takes over and from 125 °C onwards this is the dominant mechanism making C-C bonds. Moreover, even up to 75 °C, both temperature and pressure already substantially influence the selectivity and activity of the traditional CO2RR products on Cu. This study illustrates that temperature and pressure are crucial parameters to consider in applied and fundamental studies of the electrochemical reduction of CO_2.

7.2 Experimental

7.2.1 Chemicals

The electrolyte was prepared from $KHCO_3$ (99.95%, Sigma-Aldrich) with Milli-Q water (≥18.2 MΩcm, TOC < 5 ppb) and stored with Chelex (100 sodium form, Sigma-Aldrich) to clean the electrolyte from any metal impurities [52]. H_2SO_4 (95-98%, Sigma-Aldrich), H_2O_2 (35%, Merck) and $KMnO_4$ (99%, Sigma-Aldrich) were used to clean the cells. Ar (5.0 purity, Linde) and CO_2 (4.5 purity, Linde) were used for purging the electrolytes.

7.2.2 HP cell setup

We used an adapted high-pressure, high-temperature cell from Parr instruments; this cell has been described in detail in a recent paper [51]. The cell was designed to work up to 140 bar and 200 ^{0}C. The cell was used in semi-continuous mode, where either CO_2 or a mixture of CO_2 and Ar were constantly purged through the cell. The outlet of the cell was coupled to a condenser and a cooler (Cool-Care, Van der Heijden Labortechnik GMbH) to keep all volatile products in the liquid phase in the setup. The outlet gas was analyzed every 6 min with a Micro-GC from Agilent with two TCD detectors. A combination of a MS6A and a CP-PORABOND Q column was used to detect H_2, CO and CH_4, and an Al_2O_3 column was used to detect the C2 and C3 hydrocarbons. For the detection of the higher hydrocarbons, another GC with an RTX-1 column and an FID detector was used. The experimental limitation in the first part of the paper were due to the limitations of the Micro-GC which could not handle too much CO_2. Later these limitations were solved by stripping the CO_2 with NaOH before injecting the outlet gas in the GC. This allowed for the use of a pure CO_2 stream and larger injection volumes in the GC, increasing the detection limit by a factor 40. The pressure in the cell was maintained by controlling both the inlet and outlet flow with flow controllers (SLA5850, Brooks Instruments), while for the mixed gas experiments the flow was also checked with a flow meter (Defender 530+, Mesalabs). The temperature was controlled with an electric heating mantle. A homemade two-compartment PEEK cup was used inside

the stainless steel chamber and all metal parts from the thermocouple and reference electrode were covered by Teflon tape. Moreover, the lid of the vessel was covered with Viton rubber to prevent any contamination from the stainless steel.

7.2.3 General electrochemistry

The homemade PEEK cup was cleaned prior to experiments by storing in permanganate solution overnight (0.5 M H_2SO_4, 1g/L $KMnO_4$). Afterwards, the cell was rinsed, submerged in a diluted mixture of H_2SO_4 and H_2O_2 to remove any traces of MnO_4 and MnO_2, rinsed again and boiled three times with Milli-Q water. A 1mm thick Cu wire (99.99%, Mateck) was used as working electrode. Before experiments, the working electrode was electropolished in 85% H_3PO_4 (Suprapure, Merck) by applying +3 V versus a graphite counter electrode for 20 s and subsequently rinsed with Milli-Q water. Due to the large difference in current at the various conditions used, 4 different sized wires were used to ensure the current stays between 10 mA (for product detection) and 200 mA (for stability of the system) during the experiment. The areas of different working electrodes were normalized using their double layer capacitance, measured from -0.3 to 0.2 V vs SHE at scan rates from 200 to 1400 mV/s [53]. The areas of the electrodes can be found in Table S1.

During experiments, a DSA counter electrode (Magneto) was separated from the working and reference electrode by a PiperION membrane (Versogen)[54,55]. The experiments were performed with a Gamry Interface 1010B potentiostat and current interrupt[56] was used to correct for the Ohmic drop. Experiments were performed for 60 or 90 minutes at constant potential. Gaseous products were determined every 6 min with GC as described above, while liquid products were determined afterwards by sampling the 65 ml catholyte and analyzing this using high performance liquid chromatography (HPLC, Shimadzu) with an Aminex HPX-87H column (Bio-rad). During experiments the pressure was maintained within an error of 0.1 bar, while temperature was maintained within an error of 2 °C. Before reaching the conditions used for the experiment (which typically takes up to an hour), the working electrode was always under potential control at a potential of -0.8 V vs Ag/AgCl. Due to time restraints, individual experiments have not been repeated and no error bars are plotted.

7.2.4 Reference electrode corrections

In this study, all potentials are reported vs SHE(T). During experiments, an Ag/AgCl electrode (Ultradeg, 0.1 M KCl, Corr Instruments) was used as a reference electrode. However, with changing temperature, one should make several corrections to convert the potential from Ag/AgCl to SHE. The Nernst equation is used to determine the shift of the Ag/AgCl reference electrode against SHE:

$$E_{Ag/AgCl} = E^0_{Ag/AgCl}(T) - \frac{\ln(10) * RT}{nF} * \log\left(a_{Cl^-}(T)\right) \qquad (7.1)$$

with E^0 being the standard potential, R the gas constant, T the temperature, n the number of electrons, F Faradays constant and a_{Cl^-} the activity of the chloride anion. The standard potential of Ag/AgCl vs SHE is a function of temperature and can be calculated using the following formula[57]:

$$E^0_{Ag/AgCl}(T) = -0.111658 + 0.011134 * T - 0.001757268 * T * \ln(T) \qquad (7.2)$$

The temperature dependence of the activity of the chloride ions can be determined from a formula from Bogaerts et al.[58] :

$$a_{Cl^-}(T) = exp\left[\log\left(a_{Cl^-}(25\,^\circ C)\right) - \frac{\sqrt{I_{Cl^-}}}{1+\sqrt{I_{Cl^-}}} * \left(A_\gamma^T - A_\gamma^{25\,^\circ C}\right)\right] \qquad (7.3)$$

where a_{Cl^-} is the activity of the chloride anion at room temperature[59], I_{Cl} is the ionic strength of the chloride anion, and A_γ is the Debye-Huckel parameter[58].

With these formulas, the shift between an Ag/AgCl reference and SHE could be determined at different temperatures as shown in Table S2. Even though the SHE potential is defined zero at all temperatures, there is a difference in potential between SHE(T) and SHE (25°C)[60]. One could correct for this difference too, but we decide to limit the corrections to the necessary corrections and therefore report on a SHE(T) scale. In previous studies we reported on the RHE(T) scale [14,31,32,61], but in this study the potential could not be reported vs. RHE because the pH should be known to convert SHE to RHE. However, it is impossible to measure the exact pH of the electrolyte at elevated CO_2 pressures and temperatures.

7.3 Results and Discussion

7.3.1 Screening temperature, pressure and potential

As the research space increases tremendously when pressure and temperature are opened up as parameters, we first screened the effect of these parameters at different potentials. We mainly focused on -1.4 V vs SHE as shown in Figures 7.1 and F.1. This potential corresponds to -1.0 V vs RHE at ambient conditions in 0.2 M $KHCO_3$, a potential which is commonly used for electrochemical CO_2 reduction on Cu. However, we also performed screening experiments at -1.3 and -1.5 V vs SHE (Figure F.2 and F.3), as the potential can change the effects of temperature and pressure [31,61]. Experiments have been performed from 25 to 125 °C and with pressures up to 40 bar. All screening experiments were performed with 50% CO_2 and 50% Ar. Moreover, all experiments have been performed in 0.2 M $KHCO_3$

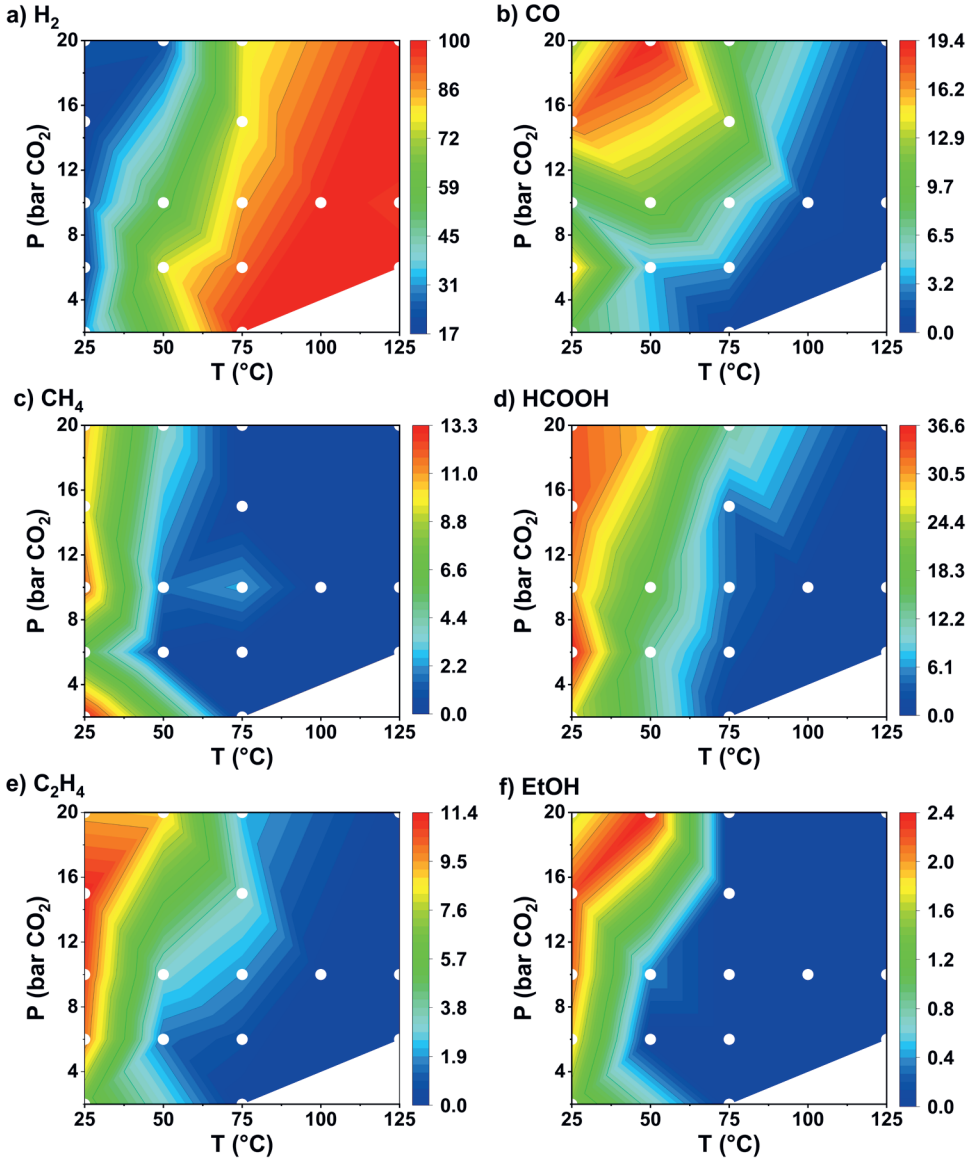

Figure 7.1 Faradaic efficiency towards the main CO2RR products as function of temperature and pressure at -1.4 V vs SHE in 0.2 M $KHCO_3$ with a 50/50 ratio of CO_2 and Ar. The white dots give the measured points and the maps are constructed via interpolation between these points. FE for a) hydrogen b) carbon monoxide c) formic acid d) methane e) ethylene and f) ethanol

because changing the electrolyte as well would increase the research space beyond reasonable measure.

Figure 7.1 shows that temperature has a more significant effect on the selectivity than pressure. With increasing temperature, more H_2 is generated and the selectivity for all CO2RR products decreases. With increasing pressure, the effect of temperature can be suppressed and the CO2RR stays active up to higher temperatures. At room temperature, there are only subtle effects on the selectivity, while the effect of pressure becomes more clear at 50 and 75 °C. These trends can also be observed at the other potentials. The exact values of the FE for the different products depends on the potential applied, but the overall trends for temperature and pressure seem independent of potential, at least in this potential window. Figure F.1 shows the 2D maps for the minor products. In general, the trends are similar to the major products in Figure 7.1, however the effect of pressure at room temperature is more clear, especially for methanol and acetate. Acetate and ethylene glycol seem to form even at very high temperatures. Moreover, we observe longer hydrocarbon formation (C3+) at the highest temperatures.

7.2 Switching mechanism at high pressure and high temperature

At the highest pressures and temperatures used in this study, above 100 °C, mainly hydrogen is produced, but also small amounts of interesting and unusual CO2RR products such as ethylene glycol, propene and butene. To detect these minor products, we have used a pure CO_2 flow which allowed for more sensitive product detection. Figure 7.2a shows the selectivity for CO2RR at temperatures up to 150 °C

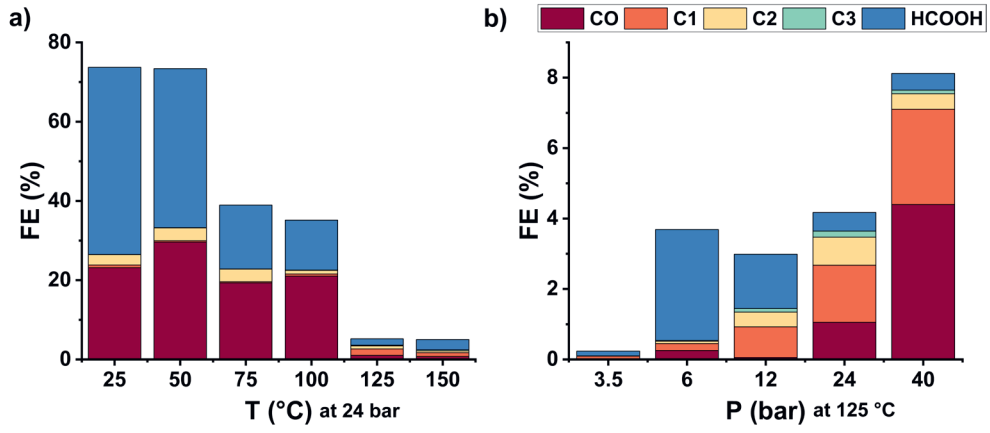

Figure 7.2 Faradaic efficiencies for the CO2RR products at function of a) temperature at 24 bar of CO_2 pressure b) pressure at 125 °C, both at -1.3 V vs SHE in 0.2 M $KHCO_3$. The remaining FE goes towards hydrogen, which is shown in Figure F.5.

at -1.3 V vs SHE. This potential was chosen as Cu is very unstable at higher overpotentials at temperatures above 100 °C, as can be seen in Figure F.4, and only produces H_2 within the total experiment time (Figure F.5b). However, at lower overpotentials some CO2RR is still possible, even at 150 °C. The product distribution changes from mainly CO and HCOOH to hydrocarbons, besides the dominant H_2 production, which is shown in Figure F.5. Figure 7.2b shows that pressure also influences the CO2RR selectivity compared to HER at 125 °C, where higher pressures lead to higher CO2RR rates and a more stable operation, as seen in Figure F.4a. The selectivity of the CO2RR products changes as well, as higher pressures lead to more CO and hydrocarbons, and less HCOOH. The selectivity has a less clear trend with potential, although a potential of -1.3 V vs SHE seems to be the optimum for hydrocarbon formation, as shown in Figure F.5b. Interestingly, the CO produced at high temperatures is mainly produced at the start of the experiment as shown in Figure F.7, while the hydrocarbons are produced throughout the measurement. This observation coincides with an significant change in the current at the start of the experiment, after which it stabilizes as shown in Figure F.4b. If only the gaseous products of the last 30 minutes are analyzed, almost no CO is produced and the optimum for the hydrocarbon formation becomes more apparent, as shown in Figure F.8.

Cu is known to be able to form C-C bonds and produce C2+ products. However, longer chain hydrocarbons are usually not observed on Cu. Either C1 or C2 hydrocarbons are formed, or C3 oxygenates, such as propionaldehyde and 1-propanol. In rare instances higher hydrocarbons have been observed before on Cu [62–64] although they are more often found on other electrochemical CO2RR catalysts [16,17,65–68], with the highest selectivities on Ni [14,15]. These longer hydrocarbons are presumed to be formed via a CH_x chain growth mechanism [15,67] similar to the thermal catalytic Fischer-Tropsch reaction, while Cu traditionally forms C-C bonds via a CO dimerization (pathway C-D-E in Figure 7.4) or carbonyl coupling mechanism (pathway F-G-E). Figure 7.2a shows that at low temperatures, mainly CO and HCOOH are formed at -1.3 V vs RHE, but also some ethylene is formed via the CO dimerization mechanism. When the temperature is increased, longer-chain products are detected and from 75 °C onwards an Anderson-Flory-Schultz (AFS) plot can be constructed, as C4 products such as butene and butane are observed. From the AFS plot in Figure 7.3, it can be seen that at 75 and 100 °C, two mechanisms are active to form C-C bonds on Cu. One is the chain growth mechanism previously observed on Ni, resulting in a linear relationship in the AFS plot. However, the C2 products do not fit this linear relationship, as they are also produced via the CO dimerization mechanism, which produces mainly ethylene, leading to a peak in the AFS plot. At 125 and 150 °C, the product distribution fits the linear relationship in the AFS plot, including the C2 products, which shows that

at these temperatures, all hydrocarbons are formed via the chain growth mechanism and the CO dimerization/carbonyl coupling mechanism has become inactive.

From the slope of the linear relationship in the AFS plot, the chain growth probability can be determined. The chain growth probability gives an indication for the product distribution, where a chain growth probability of 0 leads to only methane and a chain growth probability of 1 leads to very long hydrocarbons consisting of more than 20 carbon atoms. Figure 7.3 shows that the chain growth probability on Cu increases with increasing temperature. Table F.4 shows that pressure and potential also seem to influence the chain growth probability, decreasing with increasing pressure and higher overpotential.

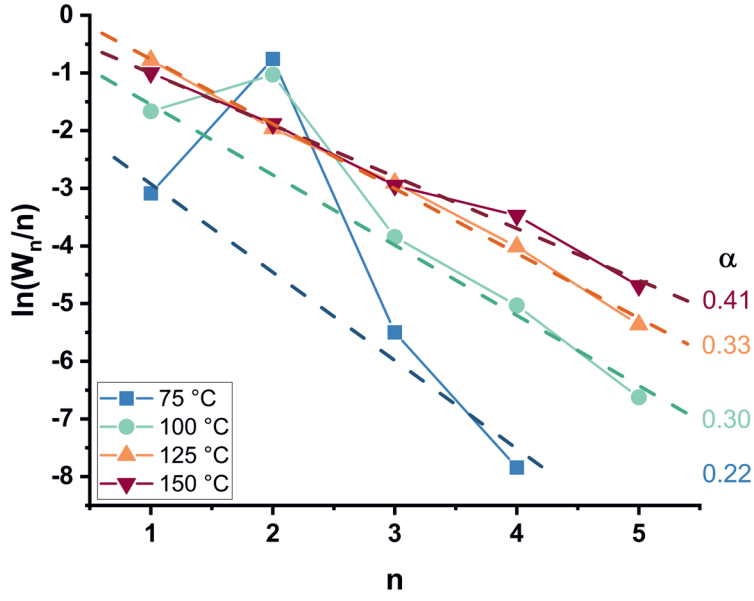

Figure 7.3 Anderson-Flory-Schultz plot (dotted lines) for Cu at -1.3 V vs SHE at 24 bar in 0.2 M $KHCO_3$ at as function of temperature. The slope of the graph gives the chain growth probability α as given on the left and in Table S3

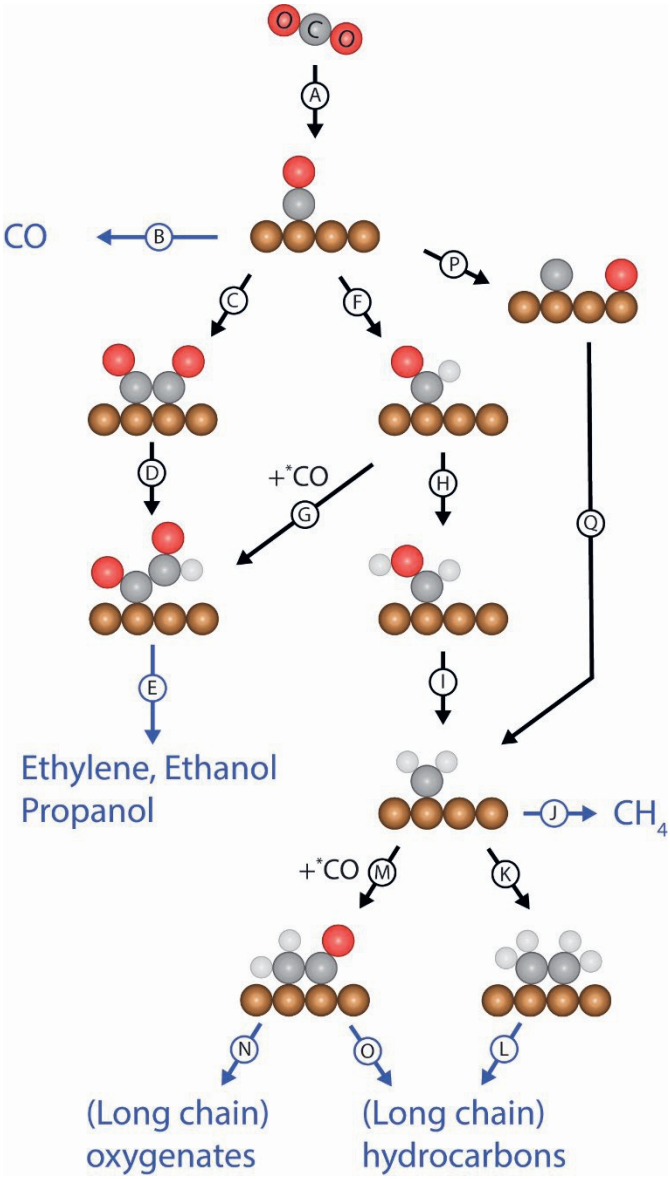

Figure 7.4 Overview of the different C-C coupling mechanisms on Cu. In blue the final products. Pathways are indicated with an arrow. We did not indicate the number of water molecules and electrons necessary for each pathway. A is the CO_2 reduction to form *CO, B the desorption of CO, C the CO dimerization and G is the carbonyl coupling to form the C-C bond. D, F, H, I and Q are the further hydrogenation of intermediates. P is the direct CO dissociation, K the CH_x coupling, M is CO insertion and E, J, L, N and O consist of multiple steps to form of the final hydrocarbons and oxygenates.

Figure 7.4 shows a overview of the different reaction pathways leading to C-C coupled products. At high temperatures the traditional C-C coupling pathways via C and G do not take place anymore as discussed above. This could be due to a lower *CO coverage, as this pathways is second order in *CO, and the *CO coverage is thus an important determinant for this pathway [69–73]. The chain growth mechanism is expected to take place via a CH_x intermediate [15,67] and would be less sensitive to the *CO coverage. Desorption of *CO (pathway B) should be faster at higher temperatures, which could lower the *CO coverage. However, we only observe little CO as product at high temperatures and only at the start of the reaction. This indicates that the *CO mostly reacts before it can desorb.

Hydrogenation is important in the chain growth mechanism and in all cases where this mechanism is observed during CO2RR, it is under conditions where HER is dominant and very little CO is formed [14,15,17,66–68]. Hydrogenation of the *CO can take place via a so-called H-assisted dissociation to form $*CH_x$ intermediates (Pathway F-H-I). Alternatively, in the thermo-catalytic Fischer-Tropsch reaction a direct dissociation of *CO is possible, which is followed by hydrogenation of the *C to form the $*CH_x$ intermediates (pathway P-Q). It might be that the latter pathway is opened up at high temperatures or that the high temperatures facilitate the fast dissociation of the *HCO. In any case, either F or P should become so fast that B and C are outcompeted. In both cases hydrogenation is important and therefore we can not distinguish between these pathways.

At low temperatures methane is already formed on Cu [7,11,73,74] via pathway F-H-I-J, but pathway M and K seem not possible as no longer hydrocarbons (apart from ethylene) have been observed. Therefore, for the chain-growth mechanism high temperatures should enhance the C-C coupling compared to CH_4 formation, as also shown by the increase in chain growth probability with temperature. The chain can grow either by CH_x coupling (Pathway K) or by CO insertion (Pathway M). It is still ambiguous which pathways is followed in the electrochemical chain-growth mechanism. However, we argue that on Cu at high temperatures the C-C bond is probably formed via CH_x coupling, because if pathway M would be active, pathway G is also expected to be active. However as discussed above, very little *CO is available, making these pathways unlikely. Moreover, pathway M should result in some oxygenates. However, neither long or short chain oxygenates have been detected at high temperatures. High temperatures should thus open up pathway K and must make this competitive to pathway J (the termination of the chain) to explain our results.

7.3 Effect of temperature

Temperature influences the stability and selectivity of Cu at temperatures much lower than 125 °C. Figure F.9 shows the effect of temperature on the FE of the major products at different pressures. These experiments were performed at -1.5 V vs SHE, as formation of C2+ products is increased at this potential. The trends at ambient pressure are very similar to the trends we reported before in a different setup [32]. However, in this study Cu is more unstable than observed before and no optimum in C2+ products with temperature is detected. Moreover, hydrogen evolution increases very rapidly with temperature, although this effect is suppressed by increasing the pressure (Figure F.11). Figure 7.5 shows the selectivity towards C_2H_4 as a function of temperature and time. Initially, at 1 bar, the effect of temperature is very similar to what we reported before. There is an optimum in ethylene selectivity at ca. 50 °C. However, in the setup used in this work the Cu seems to be less stable than before and with time the selectivity towards ethylene decreases, which gives a negative trend with temperature over the entire experiment. This electrochemical cell is very different to the design that we have used before, but also the electrode is now a wire instead of a disk, as it was previously. Additionally, the increased electrolyte concentration might explain the differences in stability. At 6 and 12 bar, similar behavior is observed, in the sense that with increasing time, the FE towards ethylene decreases. Interestingly, after 20 min, the selectivity towards ethylene remains high, even up to temperatures of 75 °C. This shows that even at a few bars of elevated pressure, formation of C2+ products can be performed at higher temperatures, most likely because the CO_2 concentration in the electrolyte is maintained at a reasonable concentration due to the increased pressure.

Figure F.12 shows the ratio in FE towards ethylene at 40 and 60 min compared to the initial FE at 20 min, as a descriptor for stability. This clearly shows that the Cu becomes less stable with increasing temperature, but increasing pressure can increase the stability. To make experiments at elevated temperatures on Cu possible, it is important to stabilize Cu at temperatures up to 75 °C, which are reasonable industrial operation temperatures [75,76], but also at higher temperatures, to utilize the chain growth mechanism discussed above. We hypothesize that the stabilization of Cu through pressure is due to the suppression of HER and an increase of the coverage of CO_2 and/or CO. However, other strategies are probably needed to obtain long term stability of the Cu catalyst at elevated temperatures. Some possible strategies may include pulsing of the potential or alloying the Cu to make it more stable at high temperatures [61].

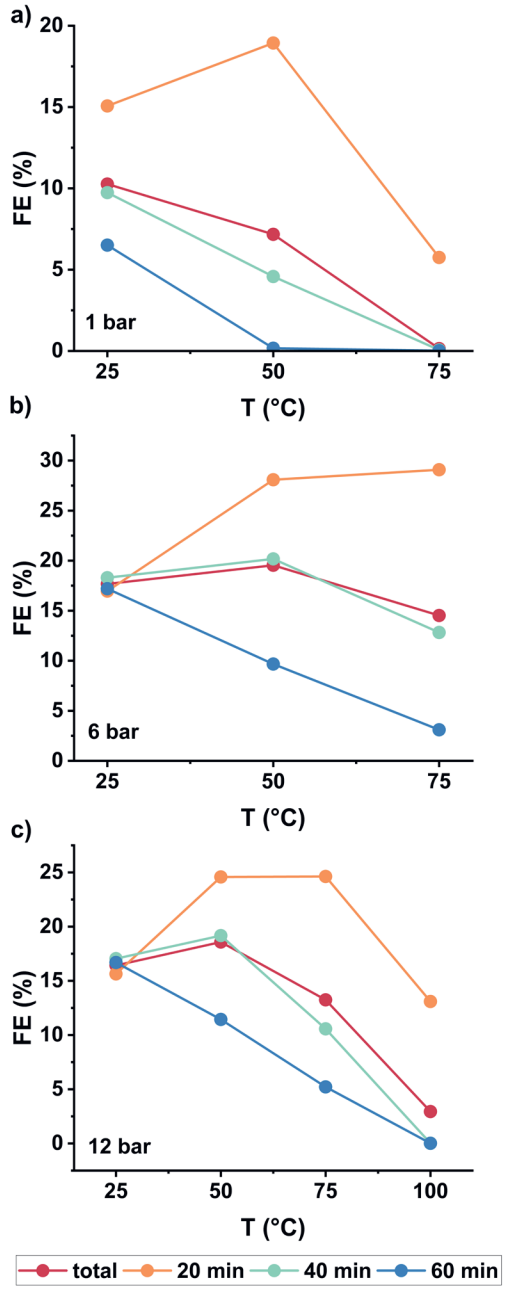

Figure 7.5 Faradaic efficiency towards ethylene as function of temperature after different electrolysis times at -1.5 V vs SHE in 0.2 M $KHCO_3$ at a) 1 bar b) 6 bar and c) 12 bar

7.4 Effect of pressure

Pressure does not only influence the stability of the Cu catalyst or increase the operating temperature window, but can itself also affect the activity and selectivity of the CO2RR. Figure 7.1 showed that the effect of pressure on the selectivity is smaller than the effect of temperature, but it is not negligible. Figure 7.6 shows the effect of pressure on the selectivity of the major products during CO2RR at -1.5 V vs SHE at room temperature, while the minor products are shown in Figure F.13. The pressure has been increased both with CO_2 and with Ar to be able to distinguish between the effect of pressure itself and of CO_2 pressure specifically.

Figures 7.6 and F.15 show that increasing CO_2 pressure can decrease the selectivity towards H_2 and that this effect already plateaus at a relatively low pressure of 3 and 6 bar at 25 and 75 °C, respectively. This same pressure is the optimum pressure for C_2H_4 selectivity, and for C2+ selectivity in general. At 25 °C, the initial pressure increase from 1 to 3 bar leads to a rapid increase in C2+ selectivity, but with further increasing pressure, the selectivity slowly decreases in favor of the simple C1 products CO and HCOOH, although the selectivity of the minor liquid products does keep increasing with increasing CO_2 pressure. Even though the selectivity towards HCOOH increases at high pressures, we never observe very selective CO2RR towards HCOOH as described in the literature [29,30]. Figure F.17 shows that this is not due to differences in electrolyte concentration between these studies.

During CO reduction on Cu, a continuous increase in C2+ selectivity with increasing pressure was observed [77,78] , which was attributed to the increasing *CO coverage. However, Figure 7.6 evidently shows this is not the case for CO_2 reduction, especially at higher pressures of 20 bar. It would be interesting to compare CO_2 and CO reduction at elevated pressures and temperatures but unfortunately, due to safety concerns, we are not able to perform CO reduction experiments at elevated pressures at this moment. Moreover, it would also be interesting to observe the *CO coverage during CO2RR at elevated pressures, which is unfortunately not possible with our current setup. However, from the product analysis, we hypothesize that the *CO coverage does not continuously increase with increasing CO_2 pressure, which might be due to faster desorption of CO due to increased CO_2 adsorption [51,79]. This limit in *CO coverage would explain the observed optimum in C2+ products at relatively low pressure and shift to simple C1 products with higher pressure.

Figure 7.6a evidently demonstrates that the suppression of H_2 at elevated pressures is due to the increase in CO_2 pressure. When the pressure is increased with Ar instead of CO_2, the FE towards H_2 increases at 25 °C, although at elevated temperatures Ar pressure does suppress HER slightly (Figure F.16a). This might be

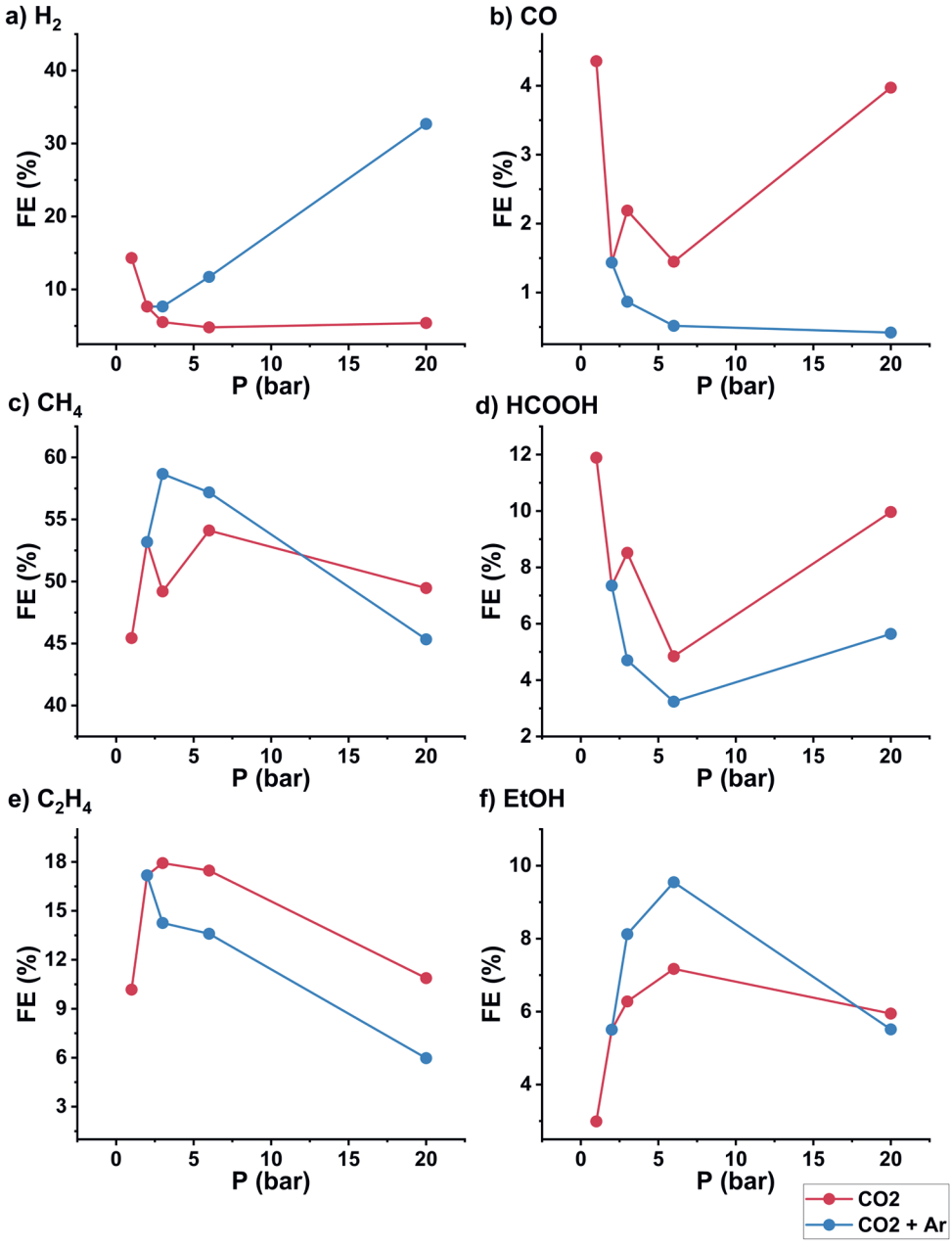

Figure 7.6 Faradaic efficiency towards the main CO2RR products as function of CO_2 and total pressure at -1.5 V vs SHE in 0.2 M $KHCO_3$ at 25 °C. Red lines are performed in pure CO_2 and blue lines are at 2 bar of CO_2 and pressure is increased with Ar. FE for a) hydrogen b) carbon monoxide c) methane d) formic acid e) ethylene and f) ethanol

due to the very high initial HER selectivity or the improved stability, even from Ar pressure. Moreover, when Ar is used to increase the pressure, most CO2RR products show lower selectivities than in a pure CO_2 atmosphere as shown in Figures 7.6 and F.13. For ethanol and methane this is not the case, but also for these products the activity is lower with Ar than in a pure CO_2 atmosphere as shown in Figure F.14 and F.16. So the increase in selectivity for these two CO2RR products is merely due to a relatively smaller decrease in activity compared to for example ethylene. These results show that the main reason for suppression of HER is not pressure itself, but CO_2 pressure, although Ar pressure might slightly help at elevated temperatures when HER is very active. We hypothesize that the HER suppression is due to competition of adsorption sides between CO_2 and H_2 intermediates, where elevated CO_2 pressures lead to less adsorption sites for HER [51].

7.4 Conclusion

In this study we have investigated the combined effect of pressure and temperature on the electrochemical CO_2 reduction on Cu. We show that temperature has a larger effect on the selectivity than pressure, although the effect of the latter is not negligible. Elevated pressures allow the performance of CO2RR at temperatures above 100 °C in aqueous systems. For the first time, we demonstrated CO2RR experiments at these high temperatures with liquid electrolytes. Although HER dominates at these conditions, we observed a change in the C-C coupling mechanism. Traditionally, C-C bonds are believed to form through a CO dimerization mechanism on Cu. However, by increasing the temperature, the chain growth mechanism, by which higher hydrocarbon chains can be formed, becomes more active, and it becomes dominant at 125 °C.

At temperatures below 100 °C, increasing the temperature can increase the FE towards traditional C2+ products and increasing the pressure can broaden the temperature range in which Cu catalysts can operate, both by increasing the CO_2 available and the Cu stability. At ambient temperature, increased CO_2 pressure itself can significantly suppress the competing hydrogen evolution reaction, even at a few bar. It is important to make the distinction between pressure and CO_2 pressure, as these do not have the same effect on the CO_2 reduction. For positive effects, it is in most cases crucial to increase the CO_2 pressure and not just the total pressure in the system.

In this study, we illustrate that temperature and pressure are crucial parameters to consider as they have significant effects both on selectivities and activities, but also on the mechanism for CO2RR. With our high-pressure, high-temperature electrochemical system we opened up the parameter space for much

broader study. This also means that there are too many parameters to investigate in this single study. In this study, all experiments were performed in 0.2 M $KHCO_3$ electrolyte, but it would be interesting to study the electrolyte effect at elevated pressures and temperatures. Moreover, it is important to study the stability of Cu at elevated pressures and especially elevated temperatures. We observe that at high temperatures, the Cu seems instable and new methods to increase the stability under these conditions must be developed. Alloying Cu with more stable metals or pulsed experiments are examples of possible ways to increase Cu stability. Furthermore, CO reduction instead of CO_2 reduction as well as experiments in different systems such as flow cell and GDE systems at both elevated pressures and temperatures are interesting and important to gain more insight into the combined effects of pressure and temperature.

References

1. Mertens, J. *et al. Joule* 7 442–449 (2023).
2. De Luna, P. *et al. Science (1979)* **364**, eaav3506 (2019).
3. Alerte, T. *et al. ACS Sustain Chem Eng* **11**, 15651–15662 (2023).
4. Roh, K. *et al. Green Chemistry* **22**, 3842–3859 (2020).
5. Bagger, A., Ju, W., Varela, A. S., Strasser, P. & Rossmeisl, J. *ChemPhysChem* **18**, 3266–3273 (2017).
6. Hori, Y. i. in *Modern aspects of electrochemistry* 89–189 (Springer, 2008).
7. Kuhl, K. P., Cave, E. R., Abram, D. N. & Jaramillo, T. F. *Energy Environ Sci* **5**, 7050–7059 (2012).
8. Kortlever, R., Shen, J., Schouten, K. J. P., Calle-Vallejo, F. & Koper, M. T. M. *Journal of Physical Chemistry Letters* **6**, 4073–4082 (2015).
9. Garza, A. J., Bell, A. T. & Head-gordon, M. (2018) doi:10.1021/acscatal.7b03477.
10. Nitopi, S. *et al. Chemical Reviews* 119 7610–7672 (2019).
11. Schouten, K. J. P., Kwon, Y., Van Der Ham, C. J. M., Qin, Z. & Koper, M. T. M. *Chem Sci* **2**, 1902–1909 (2011).
12. Kastlunger, G. *et al. ACS Catal* **12**, 4344–4357 (2022).
13. da Silva, A. H. M., Karaiskakis, G., Vos, R. E. & Koper, M. T. M. *J Am Chem Soc* **145**, 15343–15352 (2023).
14. Vos, R. E. & Koper, M. T. M. *ACS Catal* 4432–4440 (2024)
15. Zhou, Y. *et al. Nat Catal* **5**, 545–554 (2022).
16. Ma, X. & Yeo, B. S. *Current Opinion in Electrochemistry* 46 (2024).
17. Hwang, S. Y. *et al. Nano Energy* 109881 (2024)
18. da Silva, A. H. M. *et al. Journal of Electroanalytical Chemistry* **880**, (2021).
19. Jiang, K. *et al. ACS Energy Lett* **5**, 1206–1214 (2020).
20. Tang, W. *et al. Physical Chemistry Chemical Physics* **14**, 76–81 (2012).
21. Dutta, A., Rahaman, M., Luedi, N. C., Mohos, M. & Broekmann, P. *ACS Catal* **6**, 3804–3814 (2016).
22. Schouten, K. J. P., Pérez Gallent, E. & Koper, M. T. M. *Journal of Electroanalytical Chemistry* **716**, 53–57 (2014).
23. Varela, A. S., Kroschel, M., Reier, T. & Strasser, P. *Catal Today* **260**, 8–13 (2016).
24. Resasco, J., Lum, Y., Clark, E., Zeledon, J. Z. & Bell, A. T. *ChemElectroChem* **5**, 1064–1072 (2018).
25. Resasco, J. *et al. J Am Chem Soc* **139**, 11277–11287 (2017).
26. Ren, D., Fong, J. & Yeo, B. S. *Nat Commun* **9**, (2018).
27. Hara, K., Kudo, A. & Sakata, T. *Journal of Electroanalytical Chemistry* 391 (1995).
28. Hara, K., Tsuneta, A., Kudo, A. & Sakata, T. *J. Electrochem. Soc* 141 (1994).
29. Huang, L. *et al. Nat Commun* **14**, (2023).
30. Girichandran, N., Saedy, S. & Kortlever, R. *Chemical Engineering Journal* **487**, (2024).
31. Vos, R. E. & Koper, M. T. M. *ChemElectroChem* **9**, e20220023 (2022).
32. Vos, R. E. *et al. ACS Catal* **13**, 8080–8091 (2023).
33. Ahn, S. T., Abu-baker, I. & Palmore, G. T. R. *Catal Today* **288**, 24–29 (2017).

34. Hori, Y., Kikuchi, K., Murata, A. & Suzuki, S. *Chem Lett* **15**, 897–898 (1986).
35. Krause, R. *et al. Chemie Ingenieur Technik* **92**, 53–61 (2020).
36. Lobaccaro, P. *et al. Physical Chemistry Chemical Physics* **18**, 26777–26785 (2016).
37. Iglesias Van Montfort, H. P. & Burdyny, T. *ACS Energy Lett* **7**, 2410–2419 (2022).
38. Corral, D. *et al. Energy Environ Sci* **14**, 3064–3074 (2021).
39. Raaijman, S. J., Schellekens, M. P., Corbett, P. J. & Koper, M. T. M. *Angewandte Chemie - International Edition* **60**, 21732–21736 (2021).
40. Ramdin, M. *et al. Ind Eng Chem Res* **60**, 17862–17880 (2021).
41. Alerte, T. *et al. ACS Energy Lett* **6**, 4405–4412 (2021).
42. Li, J. *et al. J Am Chem Soc* **142**, 7276–7282 (2020).
43. Todoroki, M., Hara, K., Kudo, A. & Sakata, T. *Journal of Electroanalytical Chemistry* vol. 394 (1995).
44. Lamaison, S. *et al. Joule* **4**, 395–406 (2020).
45. Van Der Laan, G. P. & Beenackers, A. A. C. M. *Catal Rev Sci Eng* **41**, 255–318 (1999).
46. Van Santen, R. A., Markvoort, A. J., Filot, I. A. W., Ghouri, M. M. & Hensen, E. J. M. *Physical Chemistry Chemical Physics* **15**, 17038–17063 (2013).
47. ten Have, I. C. & Weckhuysen, B. M. *Chem Catalysis* 1 339–363 (2021).
48. Niu, J. *et al. International Journal of Hydrogen Energy* 47 9183–9200 (2022).
49. Nielsen, N. D., Jensen, A. D. & Christensen, J. M. *J Catal* **393**, 324–334 (2021).
50. Grabow, L. C. & Mavrikakis, M. *ACS Catal* **1**, 365–384 (2011).
51. da Silva, A. H. M., Vos, R. E., Schrama, R. J. C. & Koper, M. T. M. *Electrochim Acta* **498**, 144612 (2024).
52. Wuttig, A. & Surendranath, Y. *ACS Catal* **5**, 4479–4484 (2015).
53. Morales, D. M. & Risch, M. *Journal of Physics: Energy* **3**, 34013 (2021).
54. Wang, J. *et al. Nat Energy* **4**, 392–398 (2019).
55. Achrai, B. *et al. J Electrochem Soc* **167**, 134518 (2020).
56. Heenan, A. R., Hamonnet, J. & Marshall, A. T. *ACS Energy Lett* **7**, 2357–2361 (2022).
57. Öijerholm, J., Forsberg, S., Hermansson, H.-P. & Ullberg, M. *J Electrochem Soc* **156**, P56 (2009).
58. Bogaerts, W. F. & Haute, A. A. Van. *J. Electrochem. Soc.* **131**, 68–72 (1984).
59. Dash, D., Kumar, S., Mallika, C. & Mudali, U. K. *ISRN Chemical Engineering* **2012**, 1–5 (2012).
60. Bosch, R. W., Bogaerts, W. F. & Zheng, J. H. *CORROSION SCIENCE SECTION* 162 (2003).
61. Vos, R. E., Smaak, J. P. & Koper, M. T. M. *J Catal* **436**, (2024).
62. Rihm, S. D., Kovalev, M. K., Lapkin, A. A., Ager, J. W. & Kraft, M. *Energy Environ Sci* **16**, 1697–1710 (2023).
63. Shibata, H., Moulijn, J. A. & Mul, G. *Catal Letters* **123**, 186–192 (2008).
64. Lee, S., Kim, D. & Lee, J. *Angewandte Chemie* **127**, 14914–14918 (2015).
65. Dong, S. T., Xu, C. & Lassalle-Kaiser, B. *Chem Sci* **14**, 550–556 (2022).
66. Maeng, J. Y., Hwang, S. Y., Kim, S. Y., Rhee, C. K. & Sohn, Y. *J Environ Chem Eng* **12**, (2024).
67. Kim, Y. J., Maeng, J. Y., Hwang, S. Y., Rhee, C. K. & Sohn, Y. *Appl Catal B* **338**, (2023).
68. Yang, J. H. *et al. ACS Appl Mater Interfaces* **16**, 3368–3387 (2024).

69. Zhan, C. *et al. ACS Catal* **11**, 7694–7701 (2021).
70. Kong, X. *et al. Nano Lett* **22**, 3801–3808 (2022).
71. Huang, Y., Handoko, A. D., Hirunsit, P. & Yeo, B. S. *ACS Catal* **7**, 1749–1756 (2017).
72. Moradzaman, M. & Mul, G. *Journal of Physical Chemistry C* **125**, 6546–6554 (2021).
73. Liu, K. *et al. Sci Bull (Beijing)* **67**, 1042–1048 (2022).
74. Bai, H. *et al. Sci Bull (Beijing)* **66**, 62–68 (2021).
75. Lei, H., Wan, Q., Tan, S., Wang, Z. & Mai, W. *Advanced Materials* **35**, (2023).
76. Liu, X. *et al. Advanced Materials* **32**, (2020).
77. Yang, W. *et al. Journal of Energy Chemistry* **85**, 102–107 (2023).
78. Hou, J., Chang, X., Li, J., Xu, B. & Lu, Q. *J Am Chem Soc* **144**, 22202–22211 (2022).
79. De Jesús-Cardona, H., Del Moral, C. & Cabrera, C. R. *Journal of Electroanalytical Chemistry* 513 (2001).